Accessing the Frank-Kasper Phase of Block Copolymer in the Fuzzy Colloid Regime

Hsin-Lung Chen (hlchen@che.nthu.edu.tw)
National Tsing Hua University
Babak Nouri
National Tsing Hua University
Chun-Yu Chen
National Synchrotron Radiation Research Center
Yu-Shan Huang
National Synchrotron Radiation Research Center
Bradley Mansel
National Tsing Hua University

Article

Keywords: Soft Quasicrystals, Multimodal Distribution, Voronoi Cells, Laves C14 Phase, Micelles, Interparticle Interaction Energy

Posted Date: November 12th, 2020

DOI: https://doi.org/10.21203/rs.3.rs-101485/v1

Abstract

The discovery of Frank-Kasper (FK) phase in block copolymer (bcp) has prompted the progress of the field of soft quasicrystals. In principle, the formation of FK phase from the supercooled liquid phase of the bcp micelles should involve the mass transport of constituent molecules to transform the unimodal distribution of micelle size into the multimodal distribution prescribed by the volume asymmetry of the Voronoi cells in the FK phase. Here we present a new regime in which the Laves C14 phase of bcp developed below the glass transition temperature of the micelle core, where the mass transport was inhibited by the immobile block chains forming the core. The bcp micelle comprising a glassy core and a soft corona resembles the fuzzy colloid and the strong van der Waals attraction between the cores directs their organization into C14 phase to minimize the interparticle interaction energy under the metastable condition.

Introduction

Colloidal crystallization signifies the self-organization of mesoscopic particles into periodic crystalline or aperiodic quasicrystalline order and is of both fundamental and practical significance. Colloidal crystals have found vast applications in photonics, hydrogels, mechanically robust composites and templates for porous materials.[1] From the fundamental perspective, spherical colloidal particles have been exploited as the model system to explore the crystallization mechanism of atoms due to easier in-situ observation in real space, much slower ordering kinetics, and adjustable strength and range of interparticle interaction.[2]

Broadly speaking, colloidal particles cover both hard particles that retain their shape and size upon packing in the lattice and soft deformable particles such as dendrimers and the micelles formed by block copolymers and surfactants. The packing of hard spherical particles cannot fill the space entirely due to curved surface. In a colloidal system composed of hard spheres with identical size, void fraction is minimized via close packing in face-centered cubic (FCC) or hexagonal close-packed (HCP) lattice, where the former is more stable due to slightly higher positional entropy.[3–5]

Soft colloids in the melt state tend to fill the space homogeneously by the constituent molecules; therefore, these particles are deformed into polyhedrons known as the Voronoi or Wigner-Seitz cells with their geometries determined by the lattice structure.[6,7] The Voronoi cells of body-centered cubic (BCC) and FCC lattice are truncated octahedron and rhombic dodecahedron, respectively.[8] One of the most exciting discoveries of colloidal crystallization in recent years is the formation of quasicrystalline phase and the quasicrystal approximant known as the Frank-Kasper (FK) phase in soft matter, which opened the field of “soft quasicrystal”.[9,10] In contrast to the canonical lattice structures comprising only one type of Voronoi cell, FK phases are constructed by the specific packing of the distorted icosahedron cells with the coordination number of 12, 14, 15 or 16 (denoted as Z12, Z14, Z15 and Z16, respectively) in the unit cell, where each FK phase composes of at least two types of these motifs.[10,11] Since the Voronoi cells in a given FK phase may have different volume, this type of structure was thought to form only in the systems composed of nonequivalent particles with multiple size. Indeed, quasicrystals and FK phases were

initially discovered in metallic alloys composed of atoms with distinct sizes and electronic states.[11] The concept of multiple particle size was later extended to create colloidal quasicrystals by mixing nanoparticles with different sizes.[12]

The necessity of prior mixing of particles with different size was relaxed after the discovery of FK phases in single-component soft matter, including block copolymer (bcp), [13–18] surfactant[19,20] and shape amphiphile.[21–23] Though these systems compose of only one component, the basic motif of the lattice is the micelle assembled by multiple molecules. These micelles are allowed to adjust their association number and hence volume via mass transport of the constituent molecules to fit into the lattice that minimizes the total free energy.[14,24–26] In the case of conformationally asymmetric bcp, diblock foam model (DFM) shows that the packing of the unequal-sized micelles in FK s phase minimizes the total free energy comprising the interfacial free energy and the conformational free energy of the stretched block chains.[27] The redistribution of association number to yield multiple particle size makes the micellar system effectively a mixture of particles of distinct volume, though the multiplicity stems from self-adjustment via mass transport instead of intentional prior mixing. It should be noted that the redistribution of association number has to occur above the glass transition temperatures (T_g) of both constituent blocks to assure that the required mass transport can take place.

In this study, we present an exceptional scenario that Laves C14 phase was able to develop from the supercooled micellar liquid phase of a bcp below the T_g of the micellar core, where the mass transport mechanism was inaccessible. The C14 phase thus formed dissipated upon heating above the T_g of the core (T_g^{core}), implying that its stability was relevant to the vitrification of the micellar core. In contrast to the previously studied bcp micelles with fluid core and corona, the present system approached the so-called “fuzzy colloid” comprising a hard core surrounded by a soft corona, and the interaction energy between the cores plays an important role in selecting the stable packing lattice.[28,29] Our finding adds a new regime for the ordering of bcp micelles, in that the development of FK phase does not involve the mass transport and the lattice structure is governed by a hidden free energy component.

Results And Discussion

Glass transition temperatures and conformational asymmetry of the bcp. The bcp studied was a poly(2-vinyl pyridine)-*block*-poly(dimethyl siloxane) (P2VP-*b*-PDMS) with the number average molecular weights of P2VP and PDMS blocks of 2,000 and 10,000 g/mol, respectively, and the polydispersity index of 1.15 (see Figure 1 for its chemical structure). The volume fraction of P2VP in the copolymer was 0.16. The large compositional asymmetry assured that P2VP and PDMS blocks formed the core and the corona of the micelle, respectively. The T_g of P2VP block in the copolymer measured by the rheological measurement at a frequency of 10 Hz while ramping the temperature from 40 to 100 ^oC with a heating rate of 10 ^oC/min. Figure 2 displays the measured storage modulus G' and loss modulus G" as a function

of temperature. The glass transition of P2VP core was manifested by an abrupt drop of G' in the heating ramp; the T_g determined from the mid point of the observed glass transition region was ca. 65 ^oC.

The Kuhn lengths of the two constituent blocks determined by small angle neutron scattering (SANS) were b_{P2VP} = 1.46 nm and b_{PDMS} = 0.99 nm (see Supplementary Information for details), which yielded the conformational asymmetry parameter)=1.49 by considering the mass densities ρ_{2VP}=0.977 g/cm^3 and ρ_{DMS}=0.965 g/cm^3.[30] The value of e was similar to those of the bcp systems having been reported to form FK phases.[13–15,18,31–34]

Micelle ordering resolved by small angle X-ray scattering (SAXS). Figure 3(a) shows the SAXS profiles collected by heating the solvent-cast P2VP-*b*-PDMS. At the onset temperature (i.e., 30 ^oC), the SAXS curve showed a broad peak centering at 0.47 nm^{-1} along with a shoulder at 0.75 nm^{-1}. This scattering profile was fitted well by the Percus-Yevick model of polydisperse spherical particles (see Figure S2 of the Supplementary Information), indicating that the micellar entity of the bcp still retained, but the micelles exhibited only short-range order. That is, the bcp formed the micellar liquid phase. The broad hump marked by "*i=1*" was the first-order form factor maximum of P2VP core. The fact that this peak was broad and there was no discernible higher-order peaks attested that the distribution of the core size was quite broad, as manifested by the relatively large polydispersity index (=0.154) given by the ratio of the standard deviation to the mean value (= 4.77 nm) of the sphere radius assuming Schultz size distribution.

As the temperature was raised to 80 ^oC, which situated 15 ^oC above the T_g of P2VP core (T_g^{core}), the micelles organized into BCC lattice with the unit cell dimension of *a* = 22.0 nm, as evidenced by the emergence of sharp peaks with the position ratio of 1: $2^{1/2}$: $3^{1/2}$. The SAXS results suggested that the micelles developed during the solvent evaporation and subsequent drying processes were unable to undergo a fast ordering and were trapped into a metastable micellar liquid phase at 30 ^oC. Upon heating above T_g^{core}, the micelles gained sufficient mobility to proceed with the ordering into the stable BCC phase within the experimental time scale. An order-disorder transition (ODT) occurred upon further heating to T > 160 ^oC, where the BCC phase turned into a micellar liquid phase exhibiting broader interaction and form factor peaks in the SAXS curve.

The micellar liquid phase attained at high temperature persisted in the subsequent cooling cycle, as demonstrated in Figure 3(b). The copolymer sample thus cooled was then stored at 30 ^oC for prolonged annealing. Interestingly, the sample having been annealed for 60 days was found to exhibit a large number of diffraction peaks in the SAXS curve, as shown in Figure 3(b). The diffraction peaks were indexed well according to the $P6_3/mmc$ space group of hexagonal unit cell (see Table S2 and Figure S3 of the Supplementary Information) and the entire diffraction pattern was consistent with that of Laves C14 phase of other bcp systems reported previously.[14–17] The dimensions of the large hexagonal unit cell deduced from the peak positions were *a* = 37.59 nm and *c* = 61.39 nm, yielding the ratio of *c/a* = 1.633, in accord with that associated with an ideal hexagonal cell. The unit cell of the C14 phase composes of 12

particles and is filled by three types of Voronoi cells, i.e., two types of Z12 and one Z16 cells,[14] as schematically illustrated in Figure 1(d).

The present study revealed that P2VP-*b*-PDMS was another bcp system capable of forming FK phase, where the micelles in the supercooled micellar liquid phase at 30 ^{o}C underwent a slow organization to form Laves C14 phase. According to the conventional Voronoi tessellation, the 12 particles in the unit cell of C14 phase have three different volumes, with the ratio of the largest cell volume to the smallest one being 1.23. On the other hand, the micelles in the micellar liquid phase, from which the C14 phase developed, displayed unimodal size distribution. A redistribution of the association numbers of the micelles should in principle occur during the phase transition, transforming the unimodal distribution in the micellar liquid into the multimodal distribution in C14 phase.[24] However, such a symmetry breaking process was not accessible here, since the structural organization occurred at 35 ^{o}C below T_g^{core}, thereby prohibiting the mass transport required for redistributing the association number. As a matter of fact, the SAXS profiles at $q > 0.7$ nm^{-1}, which were dominated by the form factor scattering of the P2VP core, associated with micellar liquid and C14 phase were superimposable (see Figure 4), confirming that the micelle size distribution was preserved upon the phase transformation.

Strictly speaking, the unimodal distribution of micelle size in micellar liquid phase did not fit the multiplicity of the cell volume in C14 phase; nevertheless, comparing to the scenario of monodisperse particle size, the relatively high polydispersity of micelle size in the present system could be advantageous for accommodating the volume asymmetry underlying the C14 phase.[36] Moreover, the lattice formed by bcp micelles is usually distorted, where the centroids of the micelles deviate from the ideal positions due to size distribution and thermal fluctuations. There is an allowable range of distortion within which the scattering pattern still contains sufficient number of diffraction peaks (but with broadening in peak breadth) for assigning the packing structure. In the case where mass transport is forbidden, the requirement of volume asymmetry for FK phase formation can be alleviated by lattice distortion.

The C14 phase dissipated almost completely upon heating to 90 ^{o}C, as demonstrated in the temperature-dependent SAXS profiles of the C14-forming sample collected in a heating cycle shown in Figure 5. The T_{ODT} of C14 phase was ca. 25 ^{o}C higher than T_g^{core} and was much lower than the T_{ODT} of the BCC phase observed in Figure 3(a). The result suggests that the C14 phase developed here was metastable relative to BCC phase. This is understandable in that the glassy state of polymer is nonequilibrium in nature, such that the micelle was indeed a metastable entity below T_g^{core}. If the vitrification of the core did not occur in the cooling process, the micelles would have been able to adjust their association numbers (and hence sizes) in response to the change of segregation strength; in this case, BCC should have been the thermodynamically stable ordered structure along the equilibrium free energy path representing the temperature change of the structure for the micelles with fluid core and corona. On the other hand, once the micelle size was frozen in by the vitrification of the core, the system would go through another free

energy path representing the change of the structure for micelles composed of a glassy core and fluid corona. C14 phase then became the favored packing structure under this metastable condition.

Thermodynamic driving force leading to the formation of C14 phase. The key issue remained is the thermodynamic driving force leading to the formation of C14 phase at temperature $T_g^{corona} < T < T_g^{core}$. On basis of the DFM, Reddy et al. have calculated the free energy of the micelle confined within the Voronoi cells associated with various lattice structures in the polyhedral interface limit (PIL), and demonstrated that C14 phase was unstable relative to BCC, A15 and s phases.[27] In this model, the interfacial free energy governed by the surface area per unit volume of the core is coupled with the geometry of the Voronoi cell, as the core is assumed to be the affinely shrunk copy of the cell. Therefore, the interfacial free energy is directly determined by the lattice structure chosen to calculate the total free energy of the micelle. When the micelles are brought below T_g^{core}, the core geometry is arrested upon vitrification; in this case, the PIL *ansatz* is no longer applicable in that the interfacial free energy becomes a constant and does not vary with the lattice structure chosen for calculating the total free energy of the micelles in the Voronoi cell below T_g^{core}. Now the conformational free energy of the coronal block becomes the sole variable in DFM, and BCC will be the favored packing lattice for minimizing the entropic penalty arising from stretching of the coronal blocks in the Voronoi cell, provided that the micelle core arrested (e.g. from the micellar liquid phase) adopts sphere geometry.[27] Nevertheless, the micelles of P2VP-*b*-PDMS were found to organize spontaneously into C14 phase below T_g^{core}, implying that there exists a free energy component not considered explicitly in DFM.

At $T_g^{coronna} < T < T_g^{core}$, the micelle approaches the so-called “fuzzy colloid” defined by Ziherl and Kamien to describe the particle composed of a hard core and a thin soft corona such as dendrimer.[28] In the treatment of the packing problem of the fuzzy colloid, Ziherl-Kamien (Z-K) model postulated that the packing lattice is governed by the balance between two free energy components, i.e., the bulk free energy arising from the interaction between the cores which were treated as hard spheres and the surface free energy arising from the loss of orientational entropy of the chain segments constituting the corona upon overlapping with the segments associated with the neighboring particles. This model predicted that, if the corona is thin compared to the core, the bulk free energy dominates and close-packed lattice such as FCC is favored. But when the corona is sufficiently thick, A15 lattice becomes the stable packing symmetry, in that it minimizes the contact area and hence the surface free energy of the Voronoi cells with fixed volume.[28] The micelles of P2VP-*b*-PDMS however formed neither close-packed lattice nor A15 phase predicted by Z-K model.

Z-K model was originally developed to predict the packing of fuzzy colloids composed of a thin corona formed by short alkyl chains, so the conformational free energy of these short chains was not taken into account. Recently, Pansu and Sadoc extended Z-K model to include the conformational free energy change of the coronal chains attached with hard spherical particles packed in the lattice by treating the

chain as an entropic spring.[29] Moreover, the hard sphere interaction assumed in Z-K model was replaced by the van der Waals attraction in formulating the bulk free energy. As expected, the theory predicts BCC as the packing lattice that minimizes the conformational free energy. Most intriguingly, the distribution of the interparticle distance in the lattice of C14 phase was found to minimize the van der Waals interaction energy of the particles. Consequently, the fuzzy colloids prefer to organize in C14 phase once they experience strong van der Waals attraction. This theoretical prediction was consistent with the experimental finding of C14 phase in gold nanoparticles coated with hydrophobic ligands.[37]

The energy of interaction between the cores was normally neglected in treating the packing problem of bcp micelles. This is a good assumption for weaker inter-core interaction; under this condition, the calculation of the intramicellar free energy associated with the Voronoi cells is sufficient to evaluate the stability of the corresponding lattice. Once the bcp micelles fall into the fuzzy colloid regime, the interfacial free energy of the micelle becomes independent of the lattice structure; the inter-core interaction energy determined by the positions of the micelles in the lattice may then emerge as an important variable in the total free energy. Because the particles showing poor affinity to the matrix phase tend to aggregate, the van der Waals attraction between the cores of the micelles is expected to be stronger in the bcp displaying larger Flory-Huggins interaction parameter c. In other words, the contribution of the inter-core interaction energy will be particularly important in high-c bcps, where Pansu-Sadoc (P-S) model will serve as the appropriate tool for analyzing the stabilities of the packing lattices. The solubility parameters of P2VP and PDMS are 20.6 and 15.5 $MPa^{1/2}$, respectively; the large difference in their solubility parameters prescribes a large c for P2VP-*b*-PDMS. Therefore, we believe that the formation of C14 phase in P2VP-*b*-PDMS was driven mainly by the strong attractive force between P2VP cores, according to the P-S model.[29,38]

In summary, we have disclosed a new approach for generating the Laves C14 phase of bcp through accessing the fuzzy colloid regime at $T_g^{coronna} < T < T_g^{core}$. This approach is particularly plausible for bcp displaying large c, as the strong van der Waals attraction between the cores could outweigh the conformational free energy of the coronal blocks to drive the organization of the micelles into C14 phase that minimizes the interaction energy under the metastable condition. The FK phases having been disclosed for bcp thus far include σ, A15 and Laves C14 and C15 phases, with σ phase being the most common. Bates and coworkers reported the first discovery of C14 and C15 phases via thermal path dependent processes in compositionally asymmetric polyisoprene-*block*-polylactide.[14] Their work highlighted the strong effect of thermal pathway on the final structure formed. Ryu et al. investigated the ordered structure in poly(dimethylsiloxane)-*block*-poly(2,2,2- triflouroethyl acrylate) with different block ratios and detected C14 phase at the volume fraction $f_{PDMS} = 0.85$.[17] For all the systems showing C14 phase reported thus far, the quasicrystal approximant order was established via thermal treatment above the T_gs of the constituent blocks, such that the mass transport process for redistributing the association number of the micelles was accessible. The development of the Laves C14 phase in the fuzzy colloid regime unveiled here however did not involve mass transport and would hence represent a new regime for the FK phase formation in bcp.

Methods

Sample preparation. The poly(2-vinyl pyridine)-*block*-poly(dimethyl siloxane) (P2VP-*b*-PDMS) with the number average molecular weight (M_n) of P2VP and PDMS block of 2,000 and 10,000 g/mol, respectively, and polydispersity index (M_w/M_n) of 1.15 was acquired from Polymer Source, Inc. The volume fraction of P2VP calculated from the molecular weights and mass densities of the constituent blocks was 0.16. The sample for SAXS measurement was prepared by solvent casting. The copolymer sample was dissolved in toluene to form a 1.2 wt% solution in a glass vial. The vial was capped by aluminum foil with a few small holes on it to prevent fast evaporation of solvent. The capped vial was then kept on a hot plate at 70 ^oC for 7 days and then transferred into an oven equilibrated at 100 ^oC for two days to remove the solvent completely. Finally, the sample was cooled down gradually and stored at room temperature for one day before SAXS measurement.

Rheological measurement. The T_g of P2VP core of the micelle was determined by the rheological measurements performed on an Anton-Paar MCR 302 stress-controlled rheometer. A 25mm diameter cone-and-plate geometry with one-degree angle (Anton Paar CP25-1) was used due to the small sample volume requirement of 0.07 ml together with medium diameter giving a higher sensitivity to the required low strain amplitudes. The sample loading was performed by heating the rheometer stage to 180 ^oC and then added a carefully cut bubble free section of the sample followed by lowering the gap to slightly above the measurement height of 0.054 mm. The excess sample was trimmed, moved to the measurement height, and then the temperature was lowered to 40 ^oC. Initially a strain sweep measurement was performed over a strain amplitude of 0.01 to 10 % to ascertain that the linear viscoelastic range (LVER) was accessed. Heating the sample to 150 ^oC for 5-min annealing and cooling back to 40 ^oC was performed to remove any shear-induced changes during the strain sweep measurement. For subsequent oscillatory shear measurements, the strain amplitude was set to 0.02 %, within the LVER. To measure the glass transition temperature of the P2VP block, constant strain amplitude measurements at a frequency of 10 Hz were performed while ramping the temperature from 40 to 100 ^oC with a heating rate of 10 ^oC/min.

Synchrotron small angle X-ray scattering (SAXS) measurements. SAXS measurements were conduct at beamline TPS 25A1 of Taiwan Photon Source storage ring in National Synchrotron Radiation Research Center located at Hsinchu, Taiwan. The instrument configuration utilized 25 keV corresponding to wavelength 0.083 nm for 0.5 second exposure time for each measurement. Data were collected using an EIGER 16M detector mounted at three meters from sample to produce q range 0.05 to 0.5 nm^{-1}, where $q= 4\pi/\lambda\sin(\theta/2)$, θ and λ are scattering angle and X-ray wavelength respectively. All the scattering profiles were corrected by for the scatterings from air and cell.

Data availability

The data that support the findings of this study are available from the corresponding author upon request

References

1. Yanagioka, M. & Frank, C. Structure, stability and applications of colloidal crystals. *Korea Aust. Rheol. J.* **20**, 97–107 (2008).
2. Gasser, U., Weeks, E. R., Schofield, A., Pusey, P. N. & Weitz, D. A. Real-Space Imaging of Nucleation and Growth in Colloidal Crystallization. *Science* **292**, 258–262 (2001).
3. Frenkel, D. & Ladd, A. J. C. New Monte Carlo method to compute the free energy of arbitrary solids. Application to the fcc and hcp phases of hard spheres. *J. Chem. Phys.* **81**, 3188–3193 (1984).
4. Woodcock, L. V. Entropy difference between the face-centred cubic and hexagonal close-packed crystal structures. *Nature* **385**, 141–143 (1997).
5. Mau, S.-C. & Huse, D. A. Stacking entropy of hard-sphere crystals. *Phys. Rev. E* **59**, 4396–4401 (1999).
6. Singh, J. P., Walsh, S. D. C. & Koch, D. L. Brownian Dynamics of a Suspension of Particles with Constrained Voronoi Cell Volumes. *Langmuir* **31**, 6829–6841 (2015).
7. Deza, M. & Sikirić, M. D. Voronoi polytopes for polyhedral norms on lattices. *Discret. Appl. Math.* **197**, 42–52 (2015).
8. Lucarini, V. Symmetry-Break in Voronoi Tessellations. *Symmetry* **1**, 21-54 (2009).
9. Lifshitz, R. & Diamant, H. Soft quasicrystals–Why are they stable? *Philos. Mag.* **87**, 3021–3030 (2007).
10. Huang, M. *et al.* Frank-Kasper and related quasicrystal spherical phases in macromolecules. *Sci. China Chem.* **61**, 33–45 (2018).
11. Frank, F. C. & Kasper, J. S. Complex alloy structures regarded as sphere packings. I. Definitions and basic principles. *Acta Crystallogr.* **11**, 184–190 (1958).
12. Talapin, D. V. *et al.* Quasicrystalline order in self-assembled binary nanoparticle superlattices. *Nature* **461**, 964–967 (2009).
13. Lee, S., Bluemle, M. J. & Bates, F. S. Discovery of a Frank-Kasper σ Phase in Sphere-Forming Block Copolymer Melts. *Science* **330**, 349–353 (2010).
14. Kim, K. *et al.* Thermal processing of diblock copolymer melts mimics metallurgy. *Science* **356**, 520–523 (2017).
15. Zhang, J. & Bates, F. S. Dodecagonal Quasicrystalline Morphology in a Poly(styrene-b-isoprene-b-styrene-b-ethylene oxide) Tetrablock Terpolymer. *J. Am. Chem. Soc.* **134**, 7636–7639 (2012).
16. Hayashida, K., Dotera, T., Takano, A. & Matsushita, Y. Polymeric Quasicrystal: Mesoscopic Quasicrystalline Tiling in ABC Star Polymers. *Phys. Rev. Lett.* **98**, 195502 (2007).
17. Jeon, S. *et al.* Frank–Kasper Phases Identified in PDMS-b-PTFEA Copolymers with High Conformational Asymmetry. *Macromol. Rapid Commun.* **40**, 1900259 (2019).

18. Schulze, M. W. *et al.* Conformational Asymmetry and Quasicrystal Approximants in Linear Diblock Copolymers. *Phys. Rev. Lett.* **118**, 207801 (2017).
19. Liew, C. Y., Salim, M., Zahid, N. I. & Hashim, R. Biomass derived xylose Guerbet surfactants: thermotropic and lyotropic properties from small-angle X-ray scattering. *RSC Adv.* **5**, 99125–99132 (2015).
20. Kim, S. A., Jeong, K.-J., Yethiraj, A. & Mahanthappa, M. K. Low-symmetry sphere packings of simple surfactant micelles induced by ionic sphericity. *Proc. Natl. Acad. Sci.* **114**, 4072–4077 (2017).
21. Huang, M. *et al.* Selective assemblies of giant tetrahedra via precisely controlled positional interactions. *Science* **348**, 424–428 (2015).
22. Yue, K. *et al.* Geometry induced sequence of nanoscale Frank–Kasper and quasicrystal mesophases in giant surfactants. *Proc. Natl. Acad. Sci.* **113**, 14195–14200 (2016).
23. Su, Z. *et al.* Identification of a Frank–Kasper Z phase from shape amphiphile self-assembly. *Nat. Chem.* **11**, 899–905 (2019).
24. Lee, S., Leighton, C. & Bates, F. S. Sphericity and symmetry breaking in the formation of Frank–Kasper phases from one component materials. *Proc. Natl. Acad. Sci.* **111**, 17723–17731 (2014).
25. Lindquist, B. A., Jadrich, R. B., Piñeros, W. D. & Truskett, T. M. Inverse Design of Self-Assembling Frank-Kasper Phases and Insights Into Emergent Quasicrystals. *J. Phys. Chem. B* **122**, 5547–5556 (2018).
26. Kim, K. *et al.* Origins of low-symmetry phases in asymmetric diblock copolymer melts. *Proc. Natl. Acad. Sci.* **115**, 847–854 (2018).
27. Reddy, A. *et al.* Stable Frank–Kasper phases of self-assembled, soft matter spheres. *Proc. Natl. Acad. Sci.* **115**, 10233–10238 (2018).
28. Ziherl, P. & Kamien, R. D. Maximizing Entropy by Minimizing Area: Towards a New Principle of Self-Organization. *J. Phys. Chem. B* **105**, 10147–10158 (2001).
29. Pansu, B. & Sadoc, J.-F. Metallurgy of soft spheres with hard core: From BCC to Frank-Kasper phases. *Eur. Phys. J. E* **40**, 102 (2017).
30. Xie, N., Li, W., Qiu, F. & Shi, A.-C. σ Phase Formed in Conformationally Asymmetric AB-Type Block Copolymers. *ACS Macro Lett.* **3**, 906–910 (2014).
31. Gillard, T. M., Lee, S. & Bates, F. S. Dodecagonal quasicrystalline order in a diblock copolymer melt. *Proc. Natl. Acad. Sci.* **113**, 5167–5172 (2016).
32. Chanpuriya, S. *et al.* Cornucopia of Nanoscale Ordered Phases in Sphere-Forming Tetrablock Terpolymers. *ACS Nano* **10**, 4961–4972 (2016).
33. Bates, M. W. *et al.* Stability of the A15 phase in diblock copolymer melts. *Proc. Natl. Acad. Sci.* **116**, 13194–13199 (2019).
34. Takagi, H. & Yamamoto, K. Phase Boundary of Frank–Kasper σ Phase in Phase Diagrams of Binary Mixtures of Block Copolymers and Homopolymers. *Macromolecules* **52**, 2007–2014 (2019).

35. Stukowski, A. Visualization and analysis of atomistic simulation data with OVITO-the Open Visualization Tool. *Model. Simul. Mater. Sci. Eng.* **18**, 015012 (2010).
36. Cabane, B. *et al.* Hiding in Plain View: Colloidal Self-Assembly from Polydisperse Populations. *Phys. Rev. Lett.* **116**, 208001 (2016).
37. Hajiw, S., Pansu, B. & Sadoc, J.-F. Evidence for a C14 Frank–Kasper Phase in One-Size Gold Nanoparticle Superlattices. *ACS Nano* **9**, 8116–8121 (2015).
38. Jeong, J. W., Park, W. I., Kim, M.-J., Ross, C. A. & Jung, Y. S. Highly Tunable Self-Assembled Nanostructures from a Poly(2-vinylpyridine-b-dimethylsiloxane) Block Copolymer. *Nano Lett.* **11**, 4095–4101 (2011).

Declarations

Acknowledgments

This work is supported by the Ministry of Science and Technology (MOST), Taiwan under grant No. MOST 108-2221-E-007-021. The authors appreciate the beamtime of TPS BL25A provided by NSRRC in Taiwan. The authors are also indebted to Drs. Wei-Ren Chen and Kunlun Hong for their assistance in SANS measurements.

Author contributions

B.N. prepared the samples, designed and performed the SAXS experiments, analyzed the SAXS data, interpreted the results, and wrote the manuscript. C.Y.C. contributed to the SAXS configuration and the experiments. Y.S.H. contributed to the SAXS configuration and the experiments. B.M. designed and performed the rheological experiments and analyzed the rheological data. H.L.C. designed and directed the research, analyzed the data, interpreted the results, and wrote the manuscript. All authors discussed the results and commented on the manuscript.

Competing interests

The authors declare no competing interests.

Figures

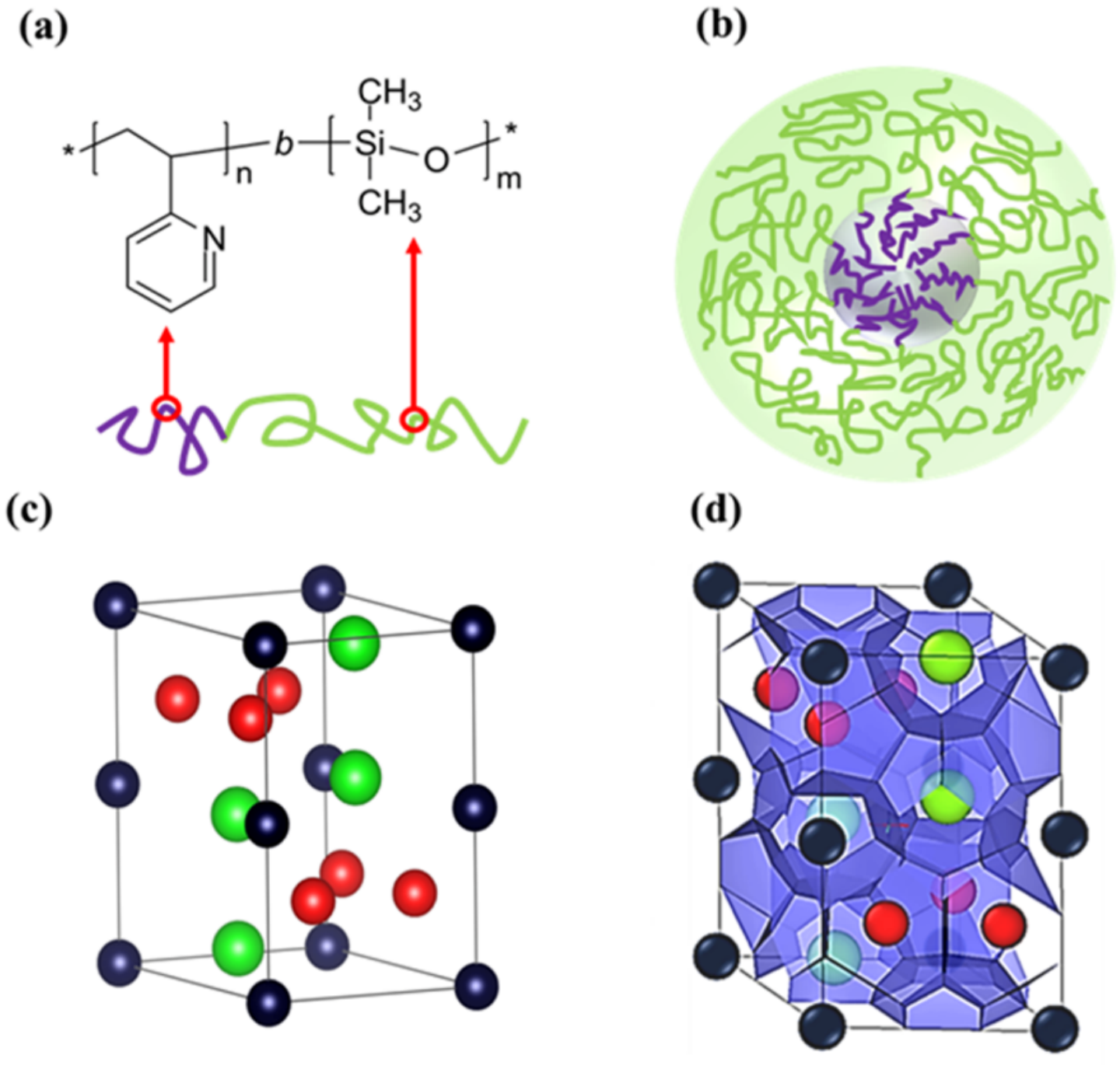

Figure 1

(a) Chemical structure of P2VP-b-PDMS; (b) schematic illustration of the micelle formed by the P2VP-b-PDMS in the native form; (c) the unit cell of Lave C14 phase (different colors represent different environment around the motifs; (d) Voronoi partitioning of the unit cell drawn by OVITO.35 The unit cell of the C14 phase composes of 12 particles and is filled by three types of Voronoi cells, i.e., two types of Z12 and one Z16 cells.

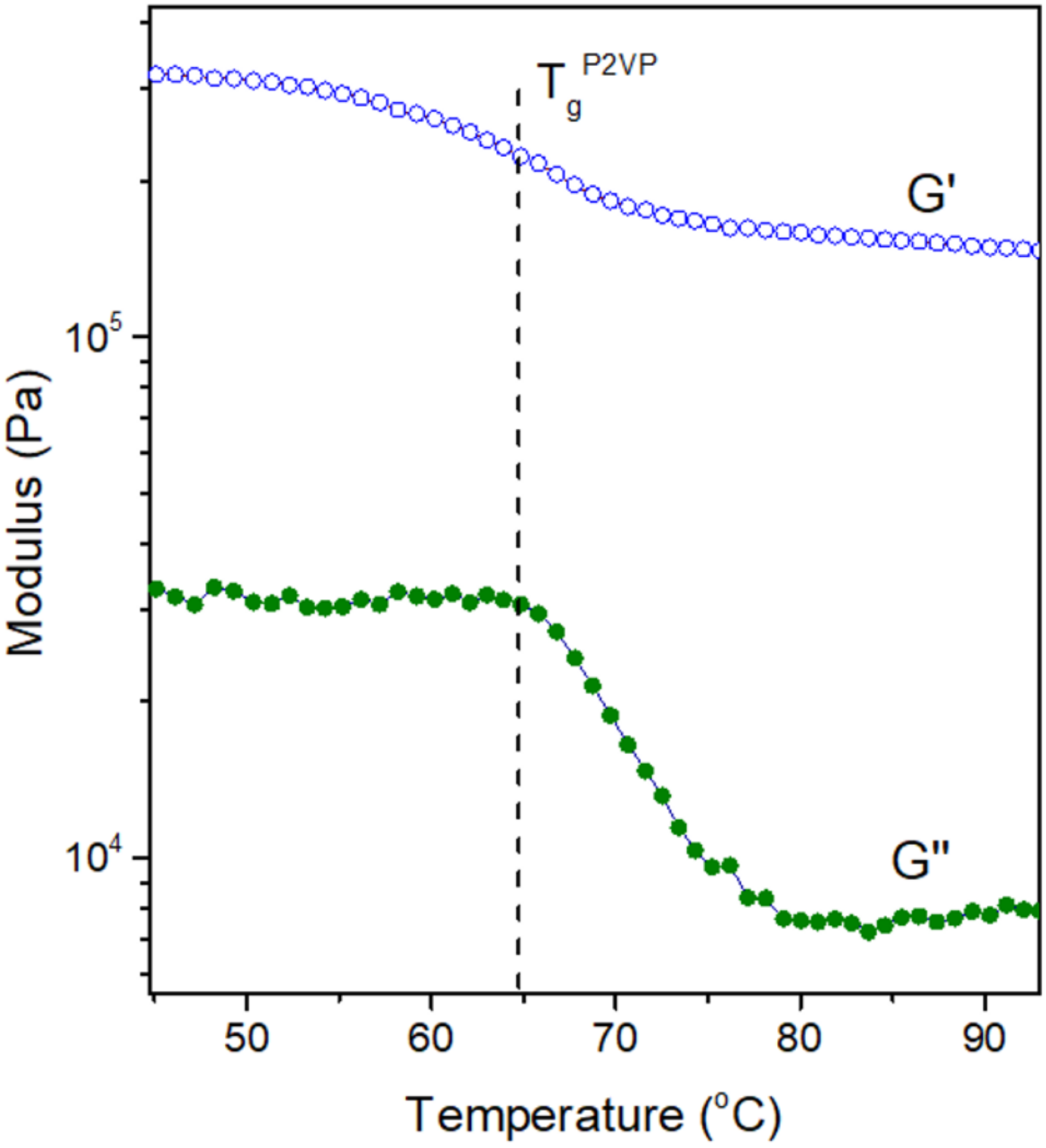

Figure 2

Results of the rheological measurement: Storage modulus G' and loss modulus G" as a function of temperature of the P2VP-b-PDMS. The measurement was performed at a frequency of 10 Hz with a heating ramp from 40 to 100 oC at 10 oC/min. The Tg of P2VP core determined from the mid point of the observed glass transition region was ca. 65 oC.

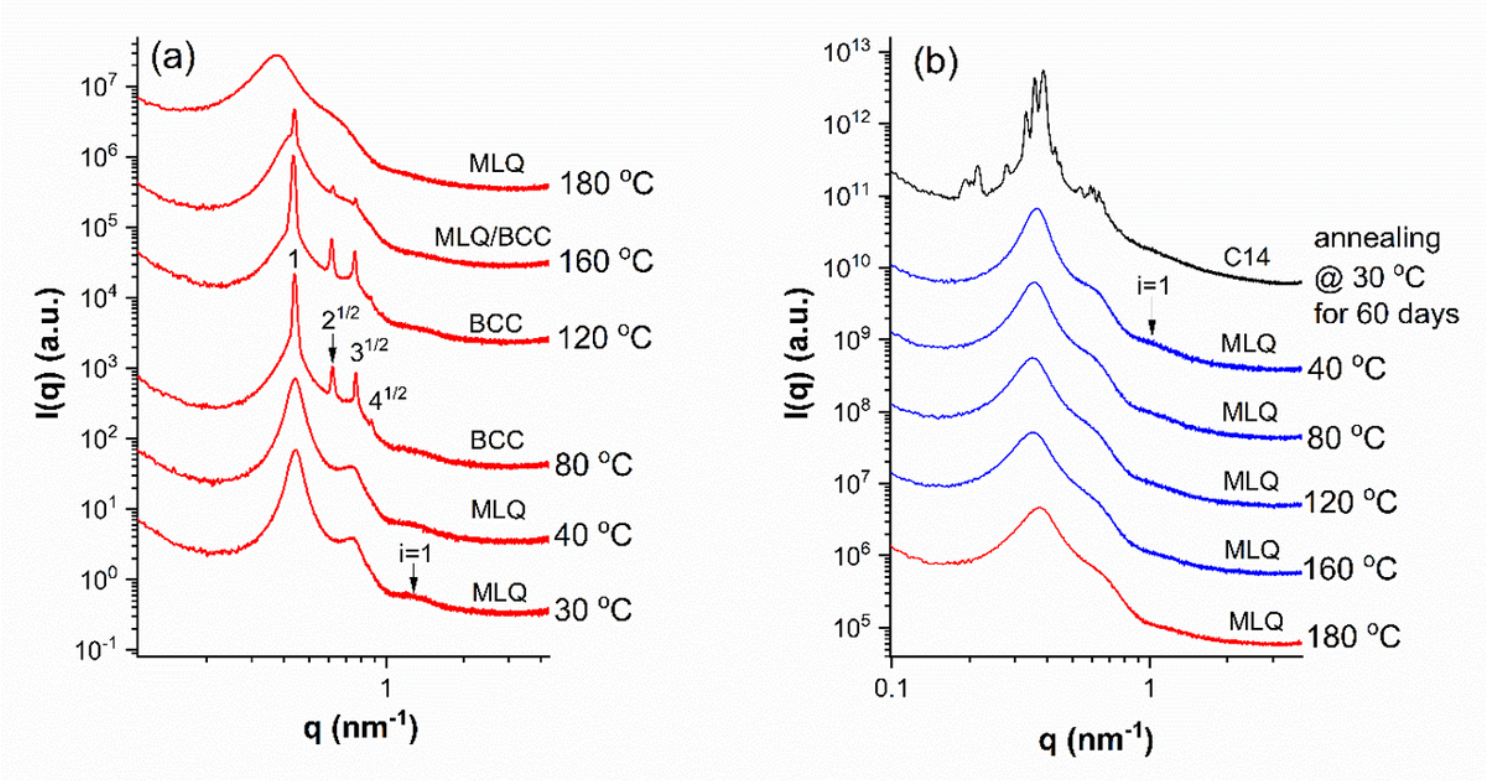

Figure 3

Temperature-dependent SAXS profiles of P2VP-b-PDMS collected in (a) a heating cycle from the as-prepared state and (b) the subsequent cooling cycle. MLQ, BCC, and C14 marked in the figure stand for micellar liquid phase, body-centered cubic packed micelles, and Laves C14 phase, respectively. The result in (b) revealed the formation of C14 phase from the micellar liquid after prolonged annealing at 30 oC for 60 days.

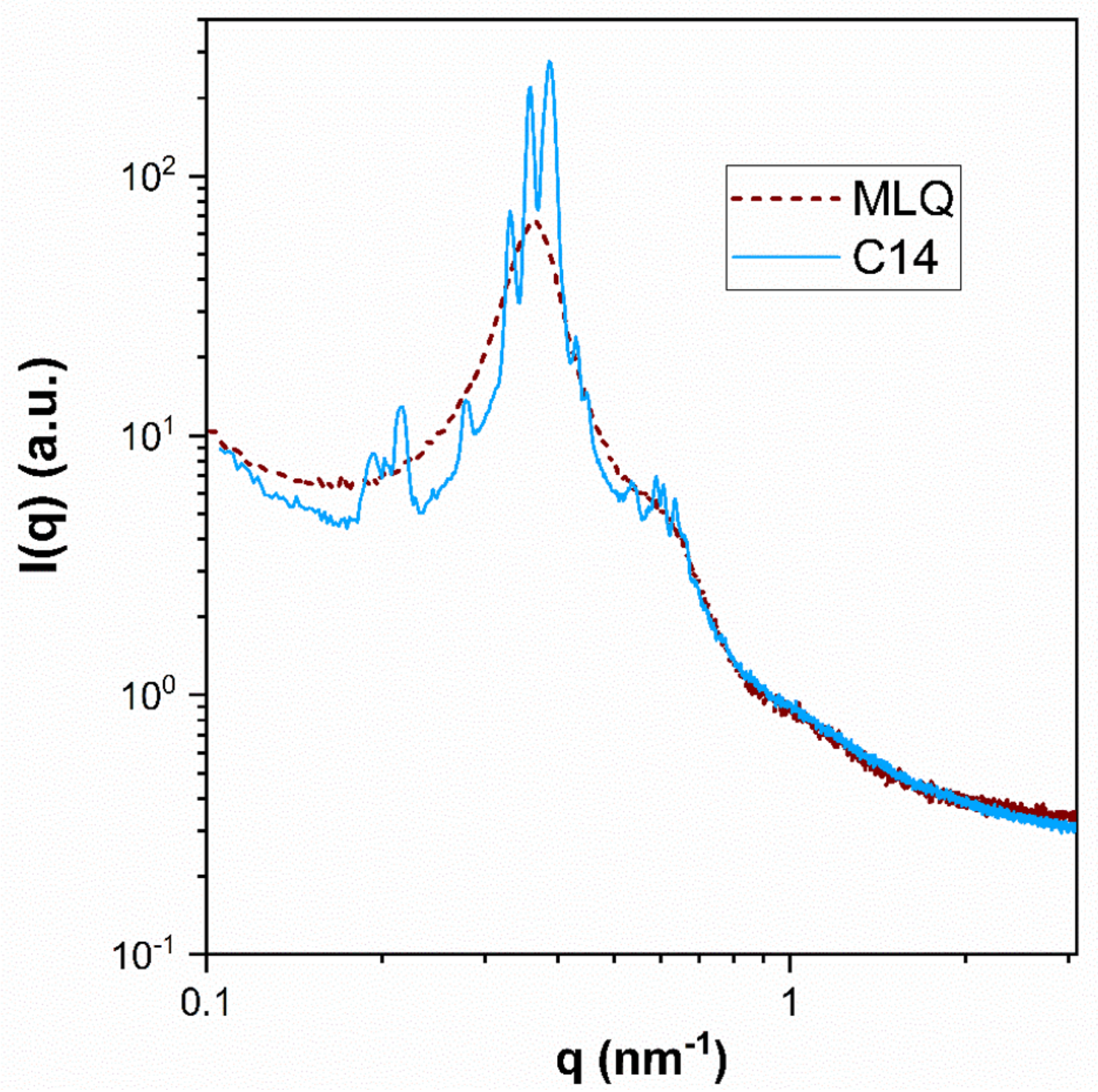

Figure 4

The SAXS profiles of the micellar liquid phase (dashed curve) and C14 phase (solid curve) developed from it. The intensity at q > 0. 7 nm-1 was dominated by the form factor scattering of the P2VP core. It can be seen that the scattering profiles associated with micellar liquid and C14 phase in this q region were superimposable, showing that the micelle size distribution was preserved upon the phase transformation.

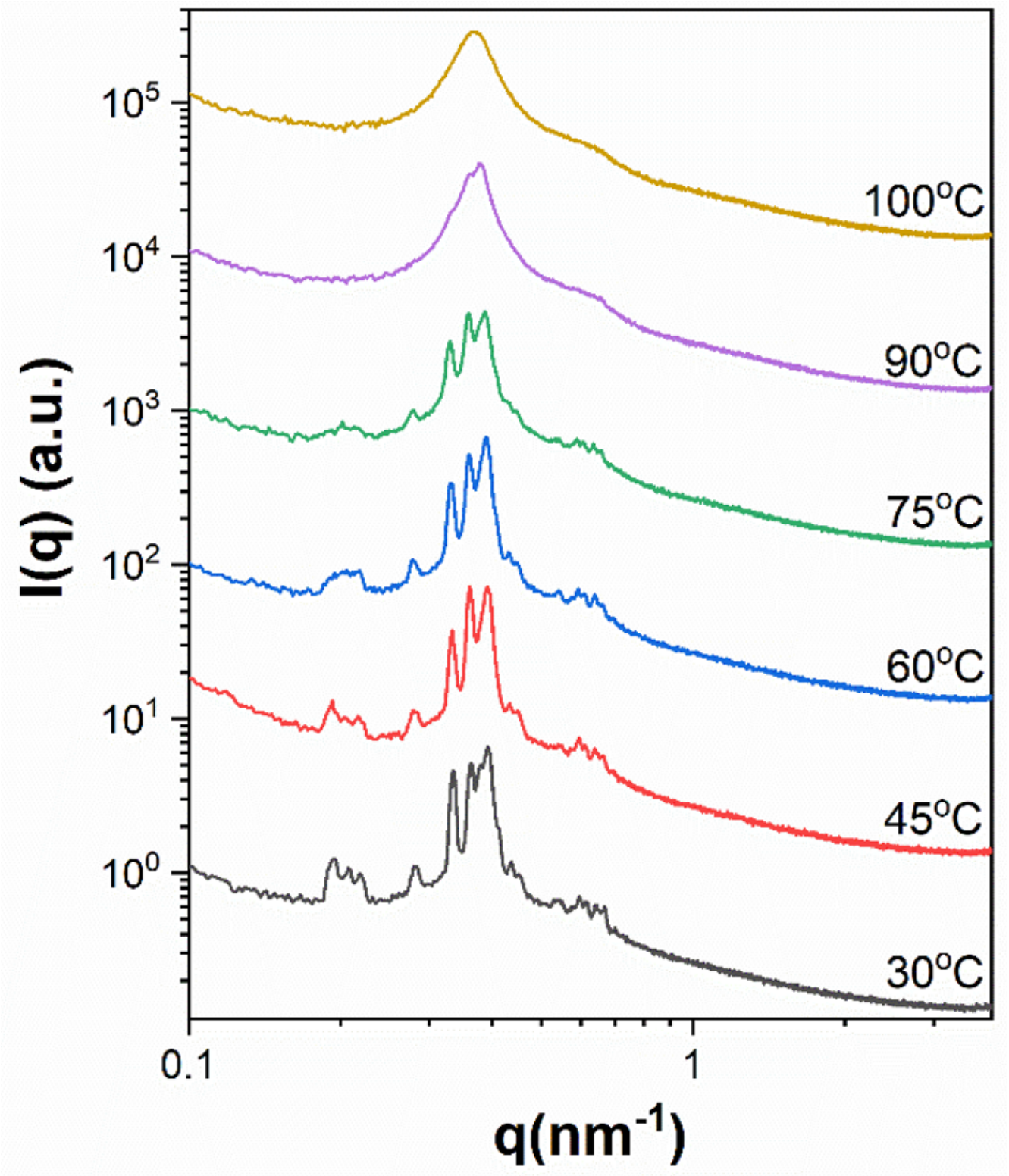

Figure 5

Temperature-dependent SAXS profiles of P2VP-b-PDMS forming the Laves C14 phase at the onset of heating. The C14 phase dissipated almost completely upon heating to 90 oC. The TODT of C14 phase was ca. 25 oC higher than Tgcore and was about 70 oC lower than that of the BCC phase observed in Figure 3(a).

Supplementary Files

This is a list of supplementary files associated with this preprint. Click to download.

- SINourietal.pdf